Title	Implication of Fluorine Atom on Electronic Properties, Ordering Structures, and Photovoltaic Performance in Naphthobisthiadiazole-Based Semiconducting Polymers
Author(s)	Kawashima, Kazuaki; Fukuhara, Tomohiro; Suda, Yousuke; Suzuki, Yasuhito; Koganezawa, Tomoyuki; Yoshida, Hiroyuki; Ohkita, Hideo; Osaka, Itaru; Takimiya, Kazuo
Citation	Journal of the American Chemical Society (2016), 138(32): 10265-10275
Issue Date	2016-07-22
URL	http://hdl.handle.net/2433/217957
Right	This document is the Accepted Manuscript version of a Published Work that appeared in final form in 'Journal of the American Chemical Society', copyright © American Chemical Society after peer review and technical editing by the publisher. To access the final edited and published work see http://doi.org/10.1021/jacs.6b05418.; The full-text file will be made open to the public on 22 July 2017 in accordance with publisher's 'Terms and Conditions for Self-Archiving'.; This is not the published version. Please cite only the published version. この論文は出版社版でありません。引用の際には出版社版をご確認ご利用ください。
Type	Journal Article
Textversion	author

Implication of Fluorine Atom on Electronic Properties, Ordering Structures, and Photovoltaic Performance in Naphthobisthiadiazole-Based Semiconducting Polymers

Kazuaki Kawashima,[1,2] Tomohiro Fukuhara,[3] Yousuke Suda,[4] Yasuhito Suzuki,[2] Tomoyuki Koganezawa,[5] Hiroyuki Yoshida,[4,6] Hideo Ohkita,[3] Itaru Osaka,[2]* and Kazuo Takimiya[1,2]*

[1]Department of Applied Chemistry, Graduate School of Engineering, Hiroshima University, 1-4-1 Kagamiya, Higashi-Hiroshima, Hiroshima 739-8527, Japan

[2]RIKEN Center for Emergent Matter Science (CEMS), 2-1 Hirosawa, Wako, Saitama 351-0198, Japan

[3]Department of Polymer Chemistry, Graduate School of Engineering, Kyoto University, Katsura, Kyoto 615-8510, Japan

[4]Graduate School of Advanced Integration Science, Chiba University, 1-33 Yayoi-cho, Inage-ku, Chiba 263-8522, Japan

[5]Japan Synchrotron Radiation Research Institute (JASRI), 1-1-1 Kouto, Sayo-cho, Sayo-gun, Hyogo 679-5198, Japan

[6]Molecular Chirality Research Center, Chiba University, 1-33 Yayoi-cho, Inage-ku, Chiba 263-8522, Japan

Abstract

The development of semiconducting polymers is imperative to improve the performance of polymer-based solar cells (PSCs). In this study, new semiconducting polymers based on naphtho[1,2-c:5,6-c′]bis[1,2,5]thiadiazole (NTz)-based polymers, PNTz4TF2 and PNTz4TF4, having 3,3′-difluoro-2,2′-bithiophene and 3,3′,4,4′-tetrafluoro-2,2′-bithiophene, respectively, are designed and synthesized. These polymers possess a deeper HOMO energy level than their counterpart, PNTz4T, which results in higher open-circuit voltages in solar cells. This concequently reduces the photon energy loss that is one of the most important issues surrounding PSCs. Whereas the PNTz4TF4 cell exhibits up to 6.5% power conversion efficiency (PCE), the PNTz4TF2 cell demonstrates outstanding device performance with as high as 10.5% PCE, which is quite high for PSCs. We further discuss the performances of the PSCs based on these polymers by correlating the charge generation and recombination dynamics with the polymer structure and ordering structure. We believe that the results would provide new insights into the design of semiconducting polymers, and that there is still much room for improvement of PSC efficiency.

Introduction

Polymer solar cells (PSCs), in which the active layer typically consists of semiconducting polymers and fullerene derivatives as p-type (hole transporting or electron donor) and n-type (electron transporting or electron acceptor) materials, respectively, have attracted considerable attention because of their solution-processability, which enables low-cost and low-environmental-impact productions.[1-3] PSCs also feature light-weight, flexibility, and semi-transparency, which potentially differentiate them from inorganic-based solar cells.[4-7] A vast number of performance improvement studies have been conducted over the past decades, which have resulted in power conversion efficiencies (PCEs) beyond 10% in single-junction cells.[8-10]

One of the most important approaches toward PCE improvement is the development of new semiconducting polymers, typically donor–acceptor (D–A) polymers wherein electron-rich (donor; D) and electron-deficient (acceptor; A) units are combined.[11-14] A narrow optical band gap (E_g) and a deep highest occupied molecular orbital (HOMO) energy level (E_H) are required for maximizing the short-circuit current density (J_{SC}) and the open-circuit voltage (V_{OC}), and thus PCE.[15] It is also desirable that the polymers have high charge carrier mobility and thus a highly crystalline structure and a favorable backbone orientation, namely, the "face-on" motif where the polymer backbones lie flat on the substrate.[16,17] Such ordering structures allow use of thick active layers, which is beneficial for light harvesting and process control.[18]

A prime example of the high-performance polymer systems is naphtho[1,2-*c*:5,6-*c*′]bis[1,2,5]thiadiazole (NTz)-based polymers, wherein NTz act as the A unit.[9,19-24] Of particular interest among the NTz-based polymers is the quaterthiophene–NTz polymer (PNTz4T) that we have previously developed (Figure 1).[20] PNTz4T possesses a narrow E_g of 1.56 eV and an E_H of −5.14 eV, and forms a relatively highly crystalline structure and face-on orientation in blend films with [6,6]-phenyl-C_{61}-butyric acid methyl ester ($PC_{61}BM$) or [6,6]-phenyl-C_{71}-butyric acid methyl ester ($PC_{71}BM$). As a result, PNTz4T demonstrates as high as 10.1% PCE, particularly with an inverted cell architecture.[9] Although

the PNTz4T cell exhibits high J_{SC}s of around 19 mA cm^{-2}, which is high for PSCs, V_{OC} is limited to 0.71–0.74 V due to the moderately deep E_H and the large photon energy loss ($E_{loss} = E_g - eV_{OC}$) of 0.82–0.85 eV, which is typical of PSCs.[25] These results have motivated us to further pursue the development of new PNTz4T-related polymers with reduced E_{loss}, i.e., with similarly narrow E_gs and deeper E_Hs.

Recently, it has been reported that the fluorine atom is a powerful functional group for semiconducting polymers.[26-32] Given its strong electron-withdrawing nature, the introduction of fluorine into the polymer backbone can deepen E_H while minimally changing E_g, resulting in the enhancement of V_{OC}. It is also believed that the fluorine atom offers non-covalent attractive interactions between the hydrogen or sulfur atoms (F···H or F···S), which may contribute to enhancing the coplanarity of the polymer backbone and therefore the crystallinity. All these features are expected to improve PSC performance.

In this work, we synthesized two new NTz-based polymers by introducing two and four fluorine atoms on the bithiophene moiety of PNTz4T, and called them PNTz4TF2 and PNTz4TF4, respectively. Whereas the PNTz4TF4 cell exhibited moderate PCE of up to 6.5%, the PNTz4TF2 cell yielded as high as 10.5% PCE. We also investigated the effects of the fluorine substitution on the electronic structure, ordering structure, photovoltaic properties, and charge generation and recombination dynamics.

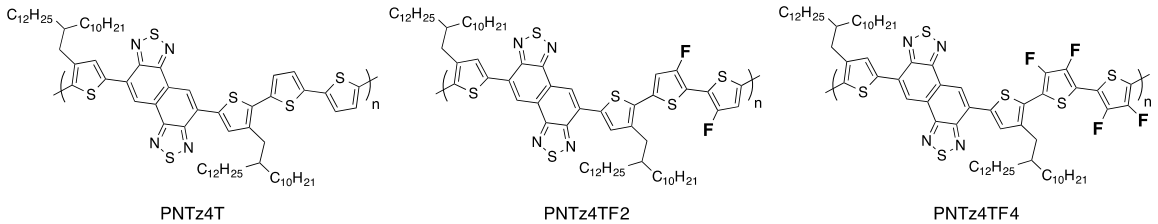

Figure 1. Chemical structures of the polymers based on NTz studied in this work.

Results

Synthesis and thermal properties of the polymers.

The key to accessing the designed polymers is the synthesis of fluorinated bithiophene compounds (Scheme 1). 5,5′-Bis(trimethylstannyl)-3,3′-difluoro-2,2′-bithiophene (**4**), the monomer of PNTz4TF2, was synthesized with a similar method that was published during our study.[29] As for the synthesis of 5,5′-bis(tributylstannyl)-3,3′,4,4′-tetrafluoro-2,2′-bithiophene (**11**), first, the α-positions of 3,4-dibromothiophene (**5**) were protected with the triisopropylsilyl (TIPS) group by lithiation using diisopropylamide (LDA) followed by treatment with chlorotriisopropylsilane to give **6** in nearly quantitative yield. Then, **6** was difluorinated to give **7** by repeating five times the lithiation with *n*-BuLi and the following treatment with *N*-fluorobenzenesulfonimide[33] in one-pot with a reasonably high yield of 88%. **7** was monoiodinated (**8**) with iodine monochloride (ICl), and then **8** was dimerized (**9**) via lithiation with *n*-BuLi followed by the oxidative coupling with copper(II) chloride ($CuCl_2$). **9** was desilylated with tetrabutylammonium fluoride (TBAF) to give **10**, which was then stannylated via lithiation with LDA and treatment with tributyltin chloride to afford **11**. Note that although the stannylation of **11** was also successful with trimethyltin chloride, the trimethyltin moiety was easily cleaved off from the resulting compound under ambient conditions.

The fluorinated monomers (**4** and **11**) were polymerized with 5,10-bis(5-bromo-4-(2-decyltetradecyl)thiophen-2-yl)naphtho[1,2-*c*:5,6-*c*′]bis[1,2,5]thiadiazole (**NTz2TBr$_2$**) via the Stille coupling reaction assisted by microwave heating to give PNTz4TF2 and PNTz4TF4, respectively. The number average molecular weight (M_n) and the weight average molecular weight (M_w) were evaluated by high-temperature gel-permeation chromatography (GPC) using *o*-dichlorobenzene (DCB) as the eluent at 140 °C. M_n and M_w were 66.5 kDa and 1520 kDa with a polydispersity index (PDI) of 22.9 for PNTz4TF2, and 15.8 kDa and 34.1 kDa with a PDI of 2.16 for PNTz4TF4, respectively (Table 1). PNTz4T was also synthesized with **NTz2TBr$_2$** and 5,5′-bis(trimethylstannyl)-2,2′-bithiophene (M_n = 52.9 kDa, M_w = 114 kDa, and PDI = 2.16).[20] The solubility of the polymers decreased as the number of

fluorine atoms increased. Because of the very low solubility, only a portion of the PNTz4TF4 solution in DCB with the typical concentration for the GPC measurement (0.67 g L^{-1}; 5×10^{-4} mol L^{-1}) was able to pass through a PTFE filter, which is technically required prior to measurement. This is most likely the reason for the low M_n of PNTz4TF4. The large PDI of 22.9 for PNTz4TF2 originates from the bimodally distributed GPC chromatogram (Figure S1), probably owing to the artifact from the strong aggregation tendency of the polymer. Such a phenomenon is sometimes seen in D–A polymers.[34] Thus, the large PDI for PNTz4TF4 may not be the real value.

Thermal properties of the polymers were evaluated by differential scanning calorimetry (DSC) (Figure S2a) and thermogravimetry (TG) (Figure S2b). Whereas the DSC curve of PNTz4T showed a melting point (T_m) at 321 °C in the heating process (302 °C in the cooling process), that of PNTz4TF2 and PNTz4TF4 showed no transition peaks below 350 °C. The DSC results suggest that the rigidity of the polymer backbone increases with the introduction of fluorine substituents. The 5% weight loss temperature (T_{d5}) determined by TG analysis were 439, 432, and 411 °C for PNTz4T, PNTz4TF2, and PNTz4TF4, respectively. These results suggest that all the polymers had good thermal stability.

Scheme 1. Synthesis of the fluorinated bithiophene monomers and polymers.

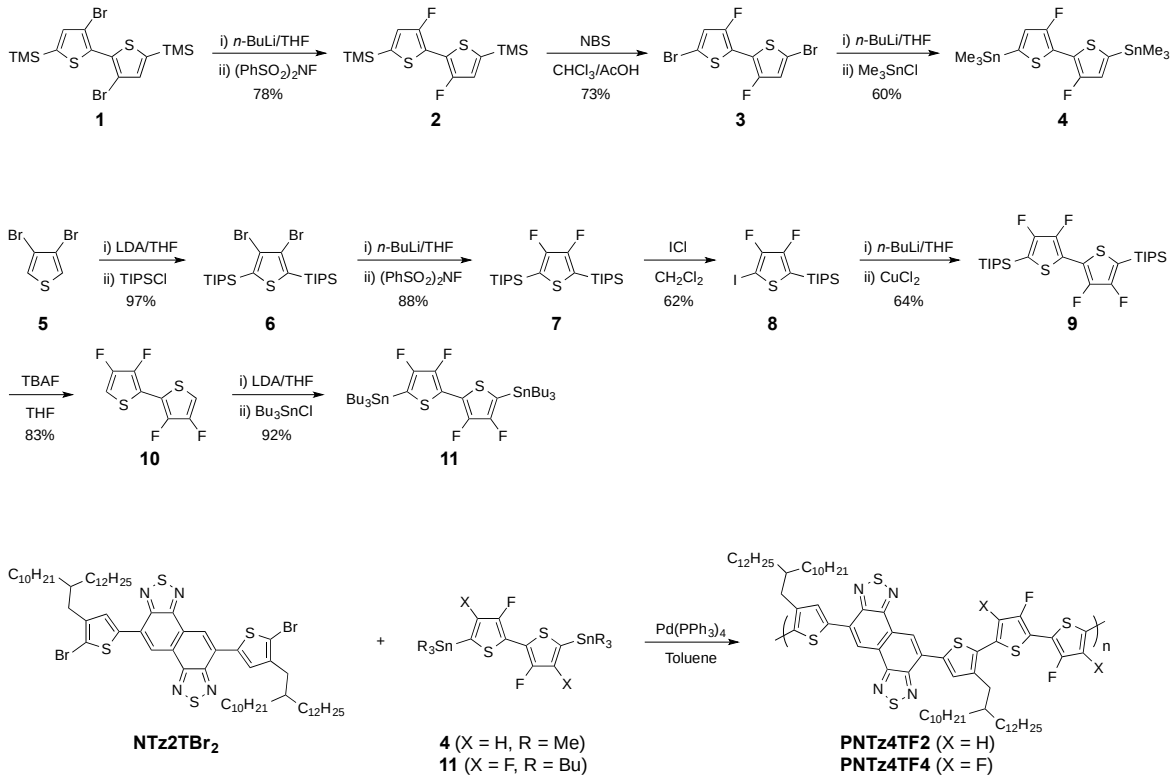

Table 1. Polymerization results.

Polymer	M_n (kDa)[a]	M_w (kDa)[a]	PDI[a]	DP_n[c]	T_m (°C)[d] heating/cooling	T_{d5} (°C)[e]
PNTz4T	52.9	114	2.16	42.5	321/302	439
PNTz4TF2	66.5	1520	22.9	52.0	–	432
PNTz4TF4	15.8[b]	34.1[b]	2.16	12.0	–	411

[a]Determined by GPC using polystyrene standard and DCB as the eluent at 140 °C. [b]Results with a fraction of the polymer solution after passing through a PTFE filter. [c]Based on the repeating unit. [d]Melting point determined by DSC measurements at the scan rate of 10 °C min^{-1}. [e] 5% weight loss temperature.

Computation and electronic properties of the polymers.

Figure 2a shows the model compounds for the polymers (dimers of the repeat units), and Figure 2b depicts the geometry-optimized structures by using the DFT method at the B3LYP/6-31g(d) level. It is obvious that the increase of fluorine substitution on the bithiophene moiety enhanced the coplanarity of the backbone as reported in other polymer systems. This well explains the low solubilities of PNTz4TF2 and PNTz4TF4 compared to that of PNTz4T. We also simply calculated the energy variation by changing the dihedral angle between the central two thiophenes (PNTz4T), fluorothiophenes (PNTz4TF2), and difluorothiophenes (PNTz4TF4), while other linkages are fixed (Figure S3). The rotation barrier from the most stable *anti* arrangement toward the *syn* arrangement was higher for PNTz4TF2 and PNTz4TF4 than for PNTz4T, implying that there are F···S attractive interactions.

The E_H values of the polymers were evaluated by photoemission yield spectroscopy (PYS) measurements in air using the thin films (Figure 3a). E_H was determined from the onset in the photoemission spectra (Table 2). E_Hs of PNTz4TF2 and PNTz4TF4 were −5.32 eV and −5.46 eV, respectively, which were deeper than that of PNTz4T (−5.15 eV) by 0.17 eV and 0.31 eV. The lowest unoccupied molecular orbital (LUMO) energy level (E_L) was evaluated by low-energy inverse photoemission spectroscopy (LEIPS)[35,36] measurements using the polymer thin films (Figure 3b). E_Ls of PNTz4TF2 and PNTz4TF4 were −3.18 eV and −3.30 eV, respectively, which were also deeper than that of PNTz4T (−3.12 eV) by 0.06 eV and 0.18 eV. These results agree well with E_Hs and E_Ls evaluated by cyclic voltammetry (CV) measurements (Table 2), which were calculated using the redox onset potentials (Figure S4, Table S1). Although E_Ls were slightly deeper when evaluated by CV, the tendency was almost the same. Note that as the energetic parameters determined by the CV measurements, which are carried out in solution, are often affected by the solvent, supporting electrolyte, and electrodes,[37] the parameters determined by the PYS and LEIPS measurements should be more reliable and closely correlated with the photovoltaic properties. It should also be mentioned that the electronic effect of the fluorine atom was larger on E_H than on E_L in this system. Figure 2b shows the

molecular orbitals computed for the model compounds, the dimer of the repeat unit with the methyl groups on thiophenes neighboring NTz, by the DFT method at the B3LYP/6-31g(d) level. LUMOs are localized on the NTz moieties whereas HOMOs are localized on the quaterthiophene moieties. It is, thus, reasonable that the fluorine atoms substituted on the quaterthiophene moieties preferencially stabilize HOMO resulting in the greater downward shift of the E_H than that of the E_L.

The UV–vis absorption spectra of the polymers were measured in chlorobenzene (CB) solution (Figure 4a) and in thin film (Figure 4b). In both PNTz4TF2 and PNTz4TF4, the absorption range and the spectral shape obtained by measurements in solution were similar to those obtained by measurements in film as in case of PNTz4T, suggesting that they aggregate, in part, even in solution. This is most likely ascribed to the strong intermolecular interaction. We also measured the absorption spectra at different temperature (20–100 °C) (Figure S5). While the spectrum of PNTz4T was largely blue-shifted with increasing the temperature, implying the disaggregation, that of PNTz4TF2 was not blue-shifted and that of PNTz4TF2 was slightly blue-shifted. This indicates that PNTz4TF2 and PNTz4TF4 have stronger aggregation tendency than PNTz4T, which is attributable to more coplanar backbones predicted by the computation. In the thin film, PNTz4TF2 and PNTz4TF4 gave rise to λ_{max} at 697 nm and 688 nm, which was bathochromically shifted by 24 nm and 33 nm relative to PNTz4T (λ_{max} = 721 nm), respectively. E_gs of PNTz4TF2 and PNTz4TF4 were calculated to be 1.60 eV and 1.62 eV from the absorption edge (λ_{edge} = 774 nm and 765 nm), respectively, and were slightly wider than that of PNTz4T (E_g =1.56 eV, λ_{edge} = 793 nm). This is consistent with their E_H and E_L values; the shift of E_H is greater than that of E_L with the introduction of fluorine.

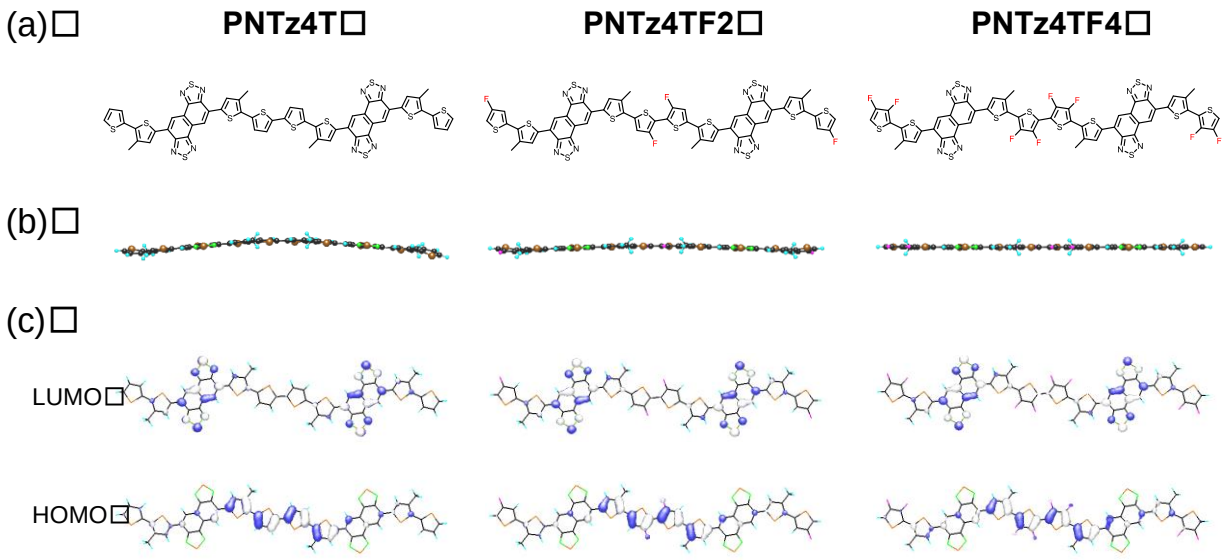

Figure 2. Chemical structure (a), optimized molecular structure (b), and geometry of HOMO and LUMO (c) for the dimer model compounds of the polymers. Calculations were carried out by the DFT method at the B3LYP/6-31G(d) level. Methyl groups were used as the side chains to simplify the calculation.

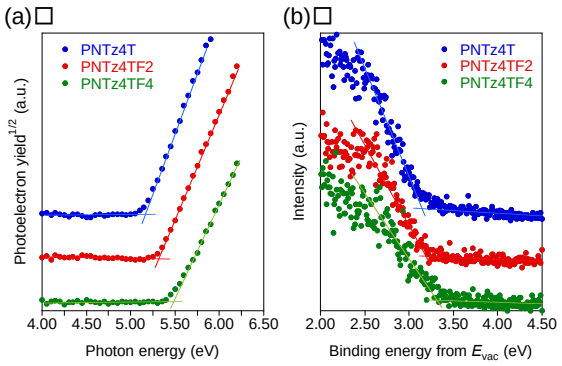

Figure 3. Photoemission yield spectra (a) and low-energy inverse photoemission spectra (b) of the polymer thin films.

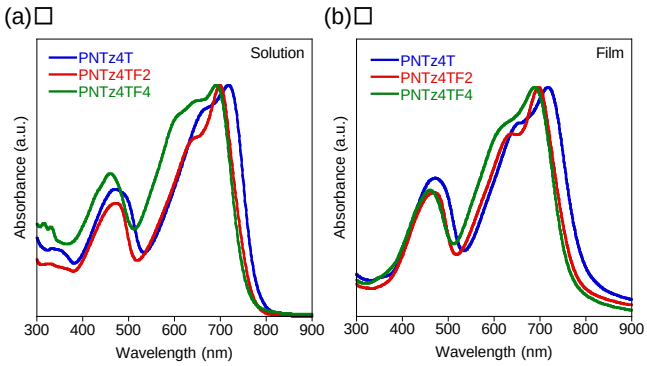

Figure 4. UV–vis absorption spectra of the polymers in chlorobenzene solution (a) and in thin film (b).

Table 2. Physicochemical properties of the polymers.

Polymer	E_H (eV)[a]		E_L (eV)[b]		λ_{max} (nm)[c]		E_g (eV)[d]
	PYS	CV	LEIPS	CV	Solution	Film	
PNTz4T	−5.15	−5.14	−3.12	−3.46	718	721	1.56
PNTz4TF2	−5.32	−5.38	−3.18	−3.53	699	697	1.60
PNTz4TF4	−5.46	−5.49	−3.30	−3.56	691	688	1.62

[a]HOMO energy levels evaluated by photoemission yield spectroscopy (PYS) in air and by cyclic voltammetry (CV). [b]LUMO energy levels evaluated by low-energy inverse photoemission spectroscopy (LEIPS) and by CV. [c]Absorption maximum. [d]Optical bandgap calculated from the absorption onset (λ_{edge}) ($E_g = 1240/\lambda_{edge}$).

Photovoltaic properties.

The photovoltaic properties of the polymers were investigated by using inverted solar cells with the indium–tin-oxide (ITO)/ZnO/(polymer/$PC_{71}BM$)/MoO_x/Ag structure. The active layer was spin-coated from the blend solution in DCB. Owing to the low solubility of the polymers at room temperature, the blend solution was heated to 100–160 °C and directly spin-coated on the substrate that was also preheated at the same temperature. The optimal polymer to $PC_{71}BM$ weight ratio (p/n ratio) was 1:2 for all the polymers.

Figures 5a and 5b depict the current density (J)–voltage (V) curves and the external quantum efficiency (EQE) spectra of the best cells, respectively, and Table 3 summarizes the photovoltaic parameters. As expected from the deeper E_H, the cells based on PNTz4TF2 and PNTz4TF4 exhibited higher V_{OC}s of 0.82 V and 0.93 V, respectively, than the PNTz4T cell. Consequently, the photon energy loss (E_{loss}), defined by $E_g - eV_{OC}$, was reduced to 0.78 eV and 0.69 eV for PNTz4TF2 and PNTz4TF4 cells, respectively, from 0.85 eV for the PNTz4T cell. Interestingly, the PNTz4TF2 cell exhibited a similar J_{SC} to the PNTz4T cell despite the fact that the range of the spectral response for the former was narrower than that of the latter as seen in the EQE spectra, reflecting their E_gs. This is due to the high EQE of the PNTz4TF2 cell (~80% in the polymer λ_{max} region) compared to that of the PNTz4T cell (~75%). Overall, although the fill factor (FF) was lower than that of the PNTz4T cells, the PNTz4TF2 cell exhibited up to 10.5% PCE (J_{SC} = 19.3 mA cm^{-2}, V_{OC} = 0.82 V, FF = 0.67), which is quite high for single-junction solar cells. Whereas V_{OC} of the PNTz4TF4 cells was the highest among the polymers studied herein, J_{SC} was significantly low (10.5 mA cm^{-2}), in good agreemente with the low EQE of ~50%, resulting in the limited PCE of 6.5%.

Figures 5c–e depict the dependence of J_{SC}, FF, and PCE on the active layer thickness (L), respectively. J_{SC} of the PNTz4TF2 cell increased as the thickness increased, reflecting the increased volume of the light-absorbing layer, and was maximum at 230 nm (Figure 5c). This behavior was similar to that of the PNTz4T cell, though the optimum thickness for the PNTz4TF2 cell was smaller than that for the

PNTz4T cell (290 nm). On the other hand, J_{SC} of the PNTz4TF4 cell reached a maximum at a much smaller thickness and significantly decreased beyond 170 nm. In all the polymer cells, FF decreased as the thickness increased, which is quite natural considering that the carriers are transported over longer distances through the electrodes. However, the decrease of FF became more significant with increasing fluorine substitution (Figure 5d). In addition, although FFs of the best cells for PNTz4TF2 (0.67) and PNTz4TF4 (0.66) were similar, these values were obtained with different active layer thicknesses of 230 nm and 120 nm, respectively. It is clear that FF of the PNTz4TF2 cell was significantly higher at similar thickness than that of the PNTz4TF4 cell. Overall, the optimal active layer thickness providing the highest PCEs was 290 nm, 230 nm, and 120 nm for PNTz4T, PNTz4TF2, and PNTz4TF4 cells, respectively (Figure 5e).

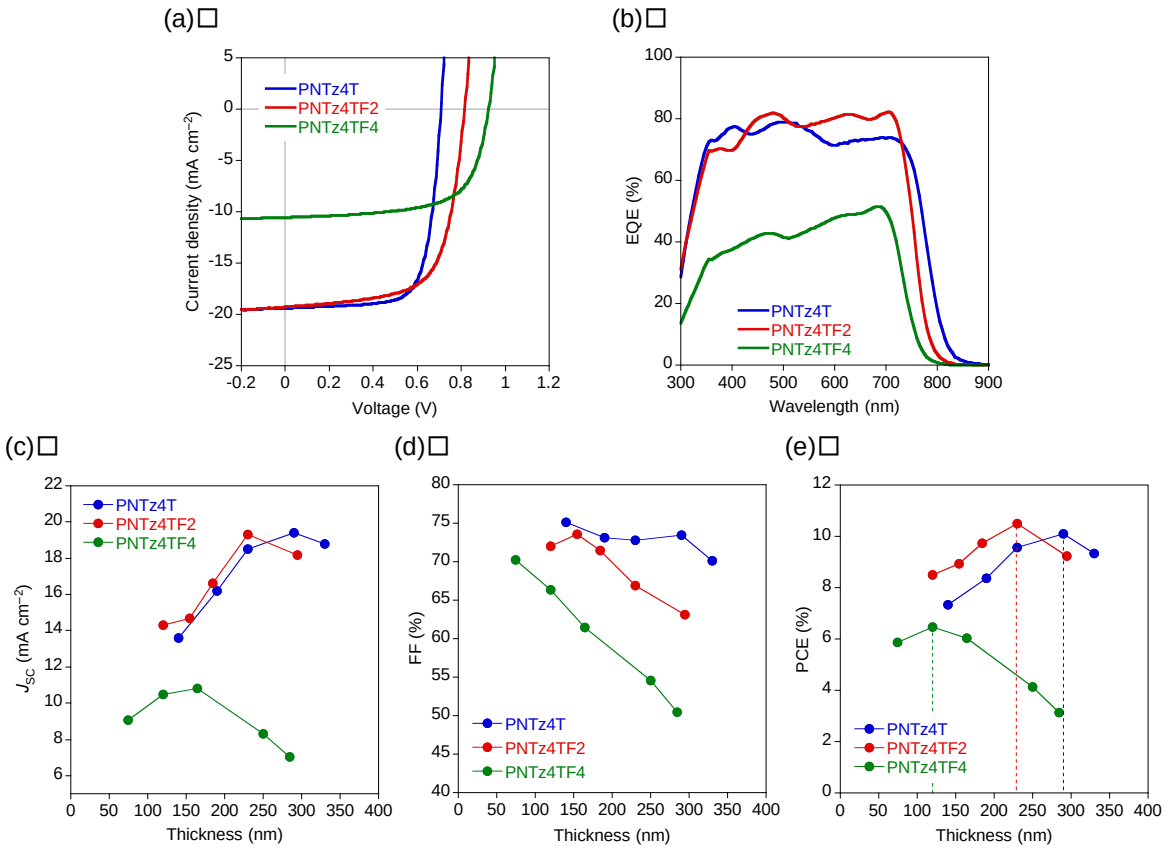

Figure 5. *J*–*V* curves (a) and EQE spectra (b) of polymer/$PC_{71}BM$ cells with the p/n weight ratio of 1:2. Thickness dependence of J_{SC} (c), FF (d), and PCE (e) of polymer/$PC_{71}BM$ solar cells.

Table 3. Photovoltaic parameters of polymer/$PC_{71}BM$ (1:2, wt ratio) solar cells.

Polymer	Thickness (nm) [a]	J_{SC} (mA cm^{-2})	V_{OC} (V)	FF	PCE_{max} [PCE_{ave}] (%) [b]	E_{loss} (eV) [c]
PNTz4T	290	19.4	0.71	0.73	10.1 [9.8±0.21]	0.85
PNTz4TF2	230	19.3	0.82	0.67	10.5 [10.1±0.25]	0.78
PNTz4TF4	120	10.5	0.93	0.66	6.5 [5.9±0.41]	0.69

[a]Thickness of the active layer. [b]PCE_{max}: maximum power conversion efficiency, PCE_{ave}: average power conversion efficiency with standard deviation for more than 20 devices. [c]Photon energy loss defined by $E_g - eV_{OC}$.

Charge transport properties of blend films.

The charge transport properties of the polymer/PCBM films in the direction normal to the substrate plane were evaluated with hole-only devices (ITO/PEDOT:PSS/(polymer/$PC_{71}BM$)/MoO_x/Ag), where the p/n ratio was 1:2 (Figure S7a). Hole mobility was calculated by using the space-charge-limited current (SCLC) model. Whereas hole mobilities of the PNTz4T and PNTz4TF2 systems were 3.4×10^{-3} and 1.5×10^{-3} cm^2 V^{-1} s^{-1}, respectively, that of the PNTz4TF4 system was 1.8×10^{-4} cm^2 V^{-1} s^{-1}, which is one order of magnitude lower (Table 4). Hole mobilities of the PNTz4T and PNTz4TF2 systems are comparable to or greater than those reported for typical high-efficiency polymer systems. To confirm the balance of charge carrier transport between hole and electron,[38] we also fabricated electron-only devices using polymer/$PC_{71}BM$ blend films (ITO/ZnO/(polymer/$PC_{71}BM$)/LiF/Al) with the p/n ratio of 1:2. The electron mobilities of all the polymer systems were of the order of 10^{-3} cm^2 V^{-1} s^{-1}: 1.1×10^{-3}, 2.1×10^{-3}, and 1.5×10^{-3} cm^2 V^{-1} s^{-1} for the PNTz4T, PNTz4TF2 and PNTz4TF4 systems, respectively (Figure S7b). Thus, whereas the hole and electron transport for the PNTz4T and PNTz4F2 systems is balanced, that for the PNTz4TF4 system is imbalanced. This imbalance would be one of the reasons for the low FF and the difficulty of using the thick active layer, and the limited PCE.

Ordering structure of the polymers.

The molecular packing and the nanostructural order of the polymers in the active layer were investigated by two-dimensional grazing incidence X-ray diffraction (2D GIXD) studies of the polymer neat film (Figure 6a–c, g–h) and polymer/$PC_{71}BM$ (p/n ratio = 1:2) blend film (Figure 6d–f, i–j) fabricated on the ZnO/ITO substrate.[39] In the polymer neat film, PNTz4T and PNTz4TF2 showed lamellar diffractions, (*h*00), along the quasi-q_z (~q_z) axis (*ca.*0.25 $Å^{-1}$), and the π–π stacking diffraction, (010), along the q_{xy} axis (around 1.8 $Å^{-1}$), indicative of the predominant edge-on orientation. On the other hand, both the lamellar and π–π stacking diffractions for PNTz4TF4 appeared as arc, suggesting the randomly oriented polymer crystallite. In the blend film, both PNTz4T and PNTz4TF2 exhibited

lamellar diffractions on both the q_{xy} and q_z axes, and the π–π stacking diffraction on the q_z axis. This indicates that these polymers predominantly orient in the face-on manner, which contrast to the polymer neat film. The π–π stacking distance (d_π) for PNTz4T and PNTz4TF2 was calculated to be 3.53 Å and 3.49 Å, respectively, which were almost the same as that in the polymer neat films. In PNTz4TF4, both the lamellar and π–π stacking diffractions were observed as a ring, indicating that the crystallites were rather randomly oriented similarly to the PNTz4TF4 neat film. Nevertheless, d_π of PNTz4TF4 was 3.46 Å, which was comparable to those of PNTz4T and PNTz4TF2.

The orientation was further studied quantitatively through the pole figure analysis using the 2D GIXD pattern of the blend films.[9,39,40] Figure 7 shows the pole figures extracted from the lamellar diffraction of the polymers, (100). We defined the areas integrated with polar angle χ ranges of 0–45° and 135–180° (A_{xy}) and 55–125° (A_z) as those corresponding to the fractions of face-on and edge-on crystallites, respectively, and the ratio of A_{xy} to A_z (A_{xy}/A_z) was calculated as a figure for the face-on to edge-on ratio. We note that A_{xy}/A_z may not show the actual face-on to edge-on ratio. A_{xy}/A_z for PNTz4TF2 was 0.62, which was lower than that for PNTz4T, namely, 0.81. This means that the population of the face-on crystallite is smaller in PNTz4TF2 than in PNTz4T. Although A_{xy}/A_z for PNTz4TF4 was 0.36, indicative of the higher edge-on ratio than PNTz4T and PNTz4TF4, we assume that again the orientation of PNTz4TF4 is rather random.

Polymer crystallinity in the blend films was also evaluated. The coherence length (L_C) of the π–π stacking structures in the face-on crystallite was estimated from the Scherrer's equation, $L_C = 2\pi/\mathrm{FWHM}$, where FWHM is the full width at half maximum of the diffraction peak (Figure S10).[41,42] The L_C value for PNTz4TF2 (29 Å) was similar to that for PNTz4T (27 Å), whereas that for PNTz4TF4 (15 Å) was approximately half those for PNTz4T and PNTz4TF2 (Table 4), despite the fact that PNTz4TF4 is expected to have the most coplanar backbone among the three polymers according to the computation (Figure 3). This could have originated in the high aggregation nature and thus the low solubility of PNTz4TF4. It is speculated that due to the low solubility, the polymer chains of PNTz4TF4

deposit quickly from the solution, which prevents the polymer chains and the crystallites being ordered, thereby resulting in the low crystallinity and the random orientation. In PNTz4T and PNTz4TF2, which have higher solubility than PNTz4TF4, would have sufficient time for self-ordering, thereby affording higher crystallinity. These differences in orientation and crystallinity among the polymers are well correlated with the charge carrier mobility and photovoltaic properties.

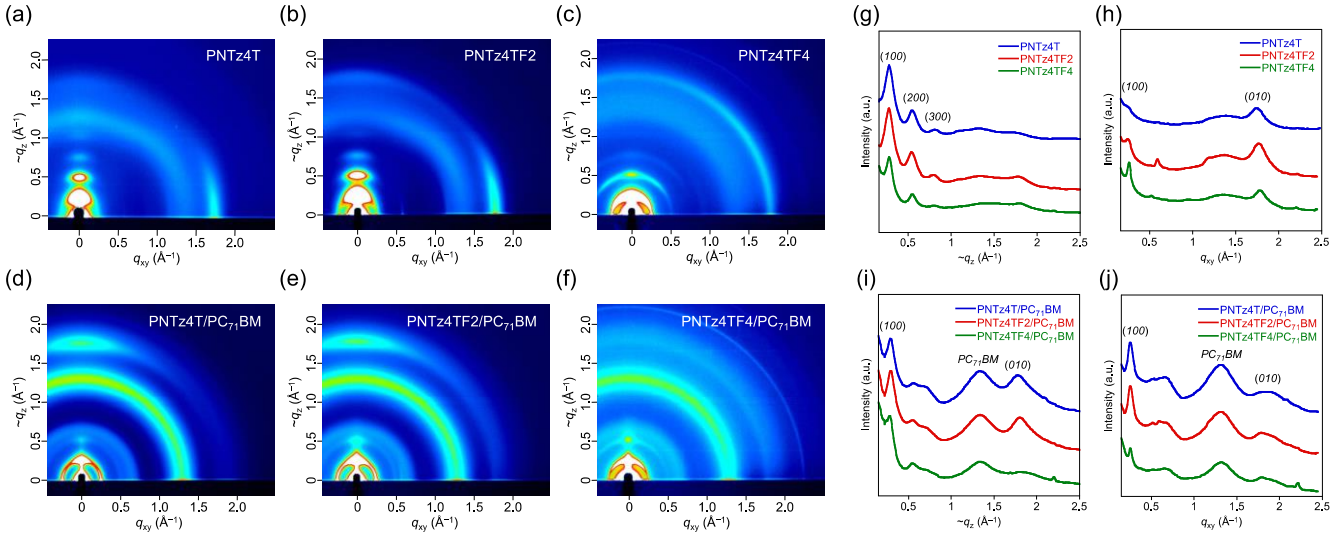

Figure 6. 2D GIXD patterns of the polymer neat films (a–c) and the polymer/$PC_{71}BM$ blend films (d–f): (a) PNTz4T, (b) PNTz4TF2, (c) PNTz4TF4, (d) PNTz4T/$PC_{71}BM$, (e) PNTz4TF2/$PC_{71}BM$, and (f) PNTz4TF4/$PC_{71}BM$. Cross-sectional profiles of the polymer neat films (g, h) and the polymer/$PC_{71}BM$ blend films (i, j) cut from the 2D GIXD patterns: (g, i) profiles along the ~q_z axis (out-of-plane) and (h, j) profiles along the q_{xy} axis (in-plane).

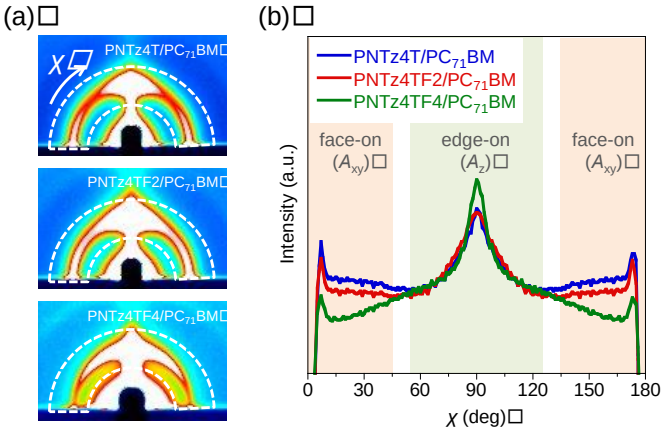

Figure 7. (a) Close-ups of the 2D GIXD patterns of the polymer/$PC_{71}BM$ blend films around the lamellar diffraction. The diffraction in the area shown by the dotted line was collected and plotted as a function of polar angle (χ). (b) Pole figure plots extracted from the lamellar diffraction in the blend films.χ ranges shown in light orange and light green correspond to the edge-on (A_z) and face-on (A_{xy}) crystallites, respectively.

Table 4. Charge carrier mobilities and parameters for the ordering structures.

Polymer	Mobility ($cm^2\ V^{-1}\ s^{-1}$)[a]		Lamellar	π–π Stacking			A_{xy}/A_z[f]
	Hole	Electron	d_l (Å)[b] [q_{xy} ($Å^{-1}$)]	d_π (Å)[c] [q_z ($Å^{-1}$)]	FWHM ($Å^{-1}$)[d]	L_C (Å)[e]	
PNTz4T	3.4×10^{-3}	1.1×10^{-3}	24.7 [0.25]	3.53 [1.78]	0.23	27	0.81
PNTz4TF2	1.5×10^{-3}	2.1×10^{-3}	24.7 [0.25]	3.49 [1.80]	0.22	29	0.62
PNTz4TF4	1.8×10^{-4}	1.5×10^{-3}	24.7 [0.25]	3.46 [1.82]	0.41	15	0.36 (random)

[a]Hole and electron mobilities evaluated with hole-only and electron-only devices, respectively, using the polymer/$PC_{71}BM$ blend films. [b]*d*-Spacing corresponds to the lamellar structure of the face-on crystallite, (100) along the q_{xy} axis. [c]*d*-Spacing corresponds to the *π–π* stacking of the face-on crystallites, (010) along the ~q_z axis. [d]Full width at half maximum for the (010) peak along the ~q_z axis. [e]Coherence length estimated from the Scherrer's equation ($L_C = 2\pi$/FWHM) for the π–π stacking of the face-on crystallite. [f]The ratio of face-on to edge-on orientation determined the pole figure analysis, where A_{xy} and A_z correspond to the face-on and edge-on fractions.

Charge generation dynamics study.

In order to discuss charge generation dynamics in the polymer/$PC_{71}BM$ blend films, we measured photoluminescence (PL) and transient absorption spectra. Figures 8a–c display the PL spectra of PNTz4T, PNTz4TF2, and PNTz4TF4 neat and polymer/$PC_{71}BM$ blend films. All the polymer neat films exhibited large PL bands at around 800 nm. On the other hand, the blend films had significantly quenched PL spectra: the quenching efficiency was estimated to be as high as >95% (PNTz4T/$PC_{71}BM$), 92% (PNTz4TF2/$PC_{71}BM$), and 90% (PNTz4TF4/$PC_{71}BM$). Such high PL quenching indicates that most of the polymer excitons are efficiently quenched to give polymer polarons before radiatively deactivating to the ground state in all the blend systems. Figure 9 shows the time evolution of the polaron bands observed for the blend films by transient absorption spectroscopy. In all cases, the polaron signals increased with a time constant of slightly less than 10 ps, which is the same as the decay constant of the polymer singlet exciton signals. These time constants are more than one order of magnitude shorter than that of the polymer singlet exciton in the polymer neat films, consistent with the highly efficient PL quenching mentioned above. At a later time stage, the polaron signals decayed with a time constant of a few hundred picoseconds for all the blend systems. This decay dynamics was independent of the excitation intensity and hence was ascribed to geminate recombination. From the constant fraction at 3000 ps, which is ascribed to dissociated free charges, the charge dissociation efficiency (η_{CD}) was estimated to be ~80% for PNTz4T/$PC_{71}BM$ and PNTz4TF2/$PC_{71}BM$ and ~50% for PNTz4TF4/$PC_{71}BM$ blend films.

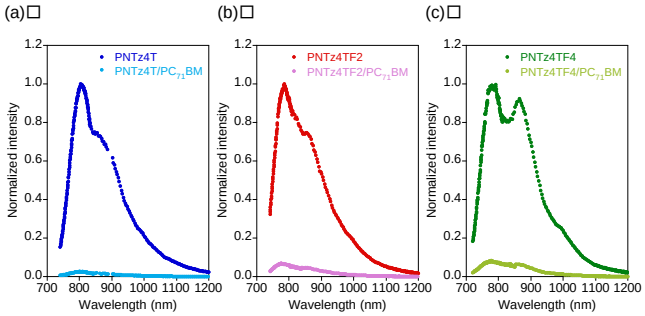

Figure 8. Normalized PL spectra. (a) PNTz4T neat and PNTz4T/$PC_{71}BM$ blend films excited at 630 nm. (b) PNTz4TF2 neat and PNTz4TF2/$PC_{71}BM$ blend films excited at 700 nm. (c) PNTz4TF4 neat and PNTz4TF4/$PC_{71}BM$ blend films excited at 690 nm.

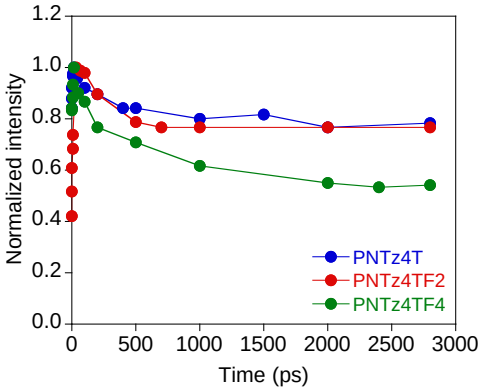

Figure 9. Normalized transient absorption of polaron signals observed for polymer/$PC_{71}BM$ blend films excited at 630 nm.

Bimolecular recombination dynamics study.

We next focused on bimolecular recombination dynamics on the microsecond time scale. The charge carrier density (n) and the charge carrier lifetime (τ_n) were evaluated by transient photovoltage (TPV) and transient photocurrent (TPC) measurements of the solar cells based on these polymers.[43,44] Figure 10a displays the dependence of the small perturbation lifetime ($\tau_{\Delta n}$) on V_{OC} obtained from the TPV measurement under different bias light intensities (from ~0.1 to 1.0 sun). In all cases, $\tau_{\Delta n}$ decreased exponentially with increasing V_{OC}, and hence was fitted by $\tau_{\Delta n} = \tau_{\Delta n0} \exp(-\beta V_{OC})$ with parameter β = 17, 19, and 22 V^{-1} for the PNTz4T, PNTz4TF2, and PNTz4TF4 systems, respectively. Figure 10b displays the dependence of n on V_{OC} obtained from the TPC measurement under different bias light intensities (from ~0.1 to 1.0 sun). As shown in the figure, charge carrier density n increased exponentially with increasing V_{OC}, which was fitted by $n = n_0 \exp(\gamma V_{OC})$ with parameter γ = 9.1, 14, and 10 V^{-1} for the PNTz4T, PNTz4TF2, and PNTz4TF4 systems, respectively. The charge carrier density n at 1 sun was thus estimated to be 2.1 × 10^{16} (PNTz4T/$PC_{71}BM$), 1.6 × 10^{16} (PNTz4TF2/$PC_{71}BM$), and 1.9 × 10^{16} cm^{-3} (PNTz4TF4/$PC_{71}BM$). As reported previously,[43,44] the charge carrier lifetime τ_n is given by $\tau_n = (1 + \lambda)\tau_{\Delta n}$ with $\lambda = \beta/\gamma$. Consequently, as shown in Figure 10c, the carrier-density dependence of τ_n is well described by a power law equation ($\tau_n = \tau_0 n^{-\lambda}$). Thus, τ_n at 1 sun was estimated to be 6.3, 3.0, and 5.6 μs for the PNTz4T, PNTz4TF2, and PNTz4TF4 systems, respectively.

On the basis of the TPV/TPC measurements, the effective bimolecular recombination coefficient (k_{rec}) is given by $k_{rec} = 1/n\tau_n$.[43-45] Under the 1 sun illumination condition, as summarized in Table 5, k_{rec} is 7.5 × 10^{-12} cm^3 s^{-1} for the PNTz4T system, which is smaller than 2.1 × 10^{-11} and 9.3 × 10^{-12} cm^3 s^{-1} estimated for the PNTz4TF2 and the PNTz4TF4 cells, respectively. On the other hand, the Langevin recombination rate is given by $k_L = q\mu/\varepsilon_0\varepsilon$, where q is the elementary charge, μ is the slower charge carrier mobility,[46] ε_0 is the vacuum permittivity, and ε is the dielectric constant. Here, μ was evaluated by the SCLC method and ε was assumed to be 3.5. Thus, k_Ls were calculated to be 5.8 × 10^{-10}, 7.9 × 10^{-10}, and 9.4 × 10^{-11} cm^3 s^{-1} for the PNTz4T, PNTz4TF2, and PNTz4TF4 systems, respectively, as

listed in Table 5. As a result, the Langevin reduction factor ($\zeta = k_{rec}/k_L$) is as low as 0.01 for PNTz4T/$PC_{71}BM$ and 0.03 for PNTz4TF2/$PC_{71}BM$, and as high as 0.1 for PNTz4TF4/$PC_{71}BM$. These results suggest that the bimolecular recombination is effectively reduced in the PNTz4T and PNTz4TF2 systems, whereas it is considered to be a Langevin recombination in PNTz4TF4/$PC_{71}BM$ blend films.

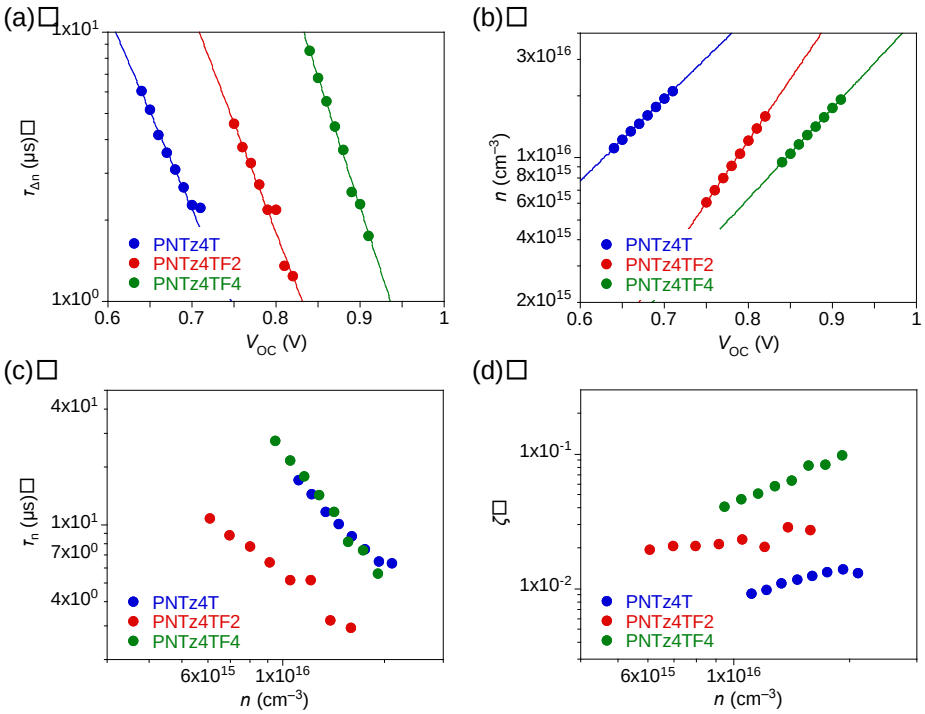

Figure 10. TPV and TPC analyses of polymer/$PC_{71}BM$ solar cells: (a) small perturbation lifetime ($\tau_{\Delta n}$) extracted from TPV measurements as a function of V_{OC}. (b) charge density (n) extracted from TPC measurements as a function of V_{OC}. (c) charge carrier lifetime (τ_n) determined from TPV and TPC measurements as a function of n. (d) Langevin reduction factor ($\zeta = k_{rec}/k_L$) as a function of n.

Table 5. Bimolecular recombination parameters of the cells

Polymer	k_{rec} ($cm^3\ s^{-1}$)[a]	k_L ($cm^3\ s^{-1}$)[b]	ζ[c]
PNTz4T	7.5×10^{-12}	5.8×10^{-10}	0.01
PNTz4TF2	2.1×10^{-11}	7.9×10^{-10}	0.03
PNTz4TF4	9.3×10^{-12}	9.4×10^{-11}	0.1

[a]Bimolecular recombination rate constant. [b]Bimolecular recombination rate constant determined by the Langevin recombination model. [c]Langevin reduction factor ($\zeta = k_{rec}/k_L$).

Discussion

We discuss herein the rationale for the device performance of the solar cells. As shown above, polymers with more fluorine atoms attached have higher V_{OC}s. This is ascribed to the deeper E_Hs of the polymers. On the other hand, J_{SC} is similar between the PNTz4T and PNTz4TF2 cells, whereas it is the lowest in the PNTz4TF4 cell. This tendency is consistent with the EQE spectra. As mentioned before, exciton quenching and polaron generation are sufficiently efficient for all the cells. In other words, the driving force is adequate for the photoinduced charge transfer at the interface even for the PNTz4TF4/$PC_{71}BM$ with the smallest LUMO–LUMO offset energy. Instead, the difference in J_{SC} and EQE is ascribed mainly to the difference in η_{CD}: it is as high as ~80% for the PNTz4T and PNTz4TF2 cells but as low as ~50% for the PNTz4TF4 cell. We speculate that such a difference in η_{CD} originates from the difference in crystallinity of the materials.[47,48] In the PNTz4T and PNTz4TF2 systems that have higher crystallinity than the PNTz4TF4 system, the generated holes and electrons can quickly diffuse away from the polymer/$PC_{71}BM$ interface, preventing the geminate recombination.

With respect to the FF and its dependence on thickness, it is likely that the charge carrier mobility and the bimolecular recombination play crucial roles. The low hole mobility, the imbalanced hole and electron transport, and the increased bimolecular recombination in the PNTz4TF4 cell relative to the PNTz4T and PNTz4TF2 cells are clear evidence of the low FF and its significant drop in thicker active layers.[49] These differences are most likely due to the difference in crystallinity and backbone orientation. Whereas PNTz4T and PNTz4TF2 had crystalline structures with the face-on orientation, which are favorable for charge transport, PNTz4TF4 was characterized by low crystallinity and a random backbone orientation.

The fact that PNTz4TF2 cell had a lower FF than the PNTz4T cell in particular at the thick active layer can be explained by the lower mobility and increased bimolecular recombination, which is likely due to the decreased fraction of the face-on crystallite in the blend film for PNTz4TF2 relative to PNTz4T, though the differences are small. To further confirm the effect of bimolecular recombination,

we calculated the bimolecular recombination current density, J_{BR}, which is given by $J_{BR} = -qLn/\tau_n$. As reported previously,[50] photocurrent density $J(V)$ can be expressed as $J(V) = J_{GEN}(V) + J_{BR}(n,V)$ where $J_{GEN}(V)$ is the free charge generation current density (the details are available in Supporting Information). As shown in Figure 11, the J–V curves can be well reproduced by this equation with charge carrier parameters obtained from TPV/TPC measurements. This finding indicates that the bimolecular recombination loss is indeed less in the PNTz4T cell, as shown in Figure 11b, consistent with the reduced recombination with a smaller ζ than in the PNTz4TF2 cell.

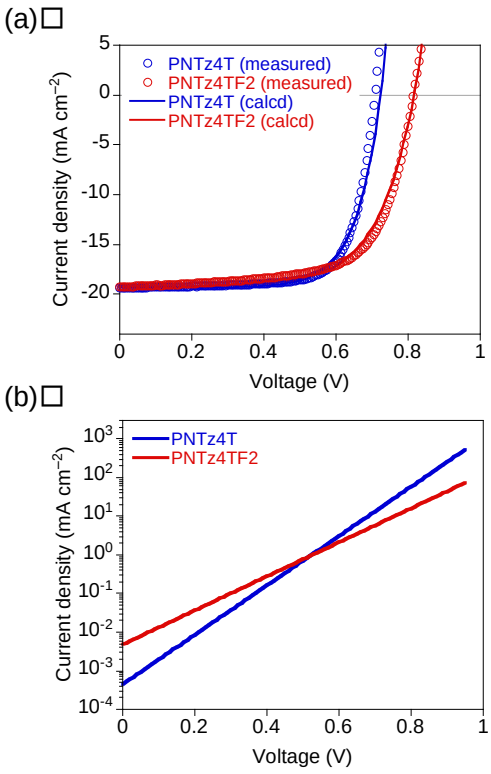

Figure 11. Comparison of the measured and calculated J–V curves (a) and bimolecular recombination current (J_{BR}) plotted against bias voltage (b) of the solar cells based on PNTz4T and PNTz4TF2.

Conclusion

We have synthesized two novel NTz-based polymers with fluorinated bithiophene units, namely, PNTz4TF2 and PNTz4TF4. The fluorination preferentially stabilized the HOMO of the polymers, resulting in larger E_{HS}, slightly larger E_{LS}, and slightly wider E_{g}s for PNTz4TF2 and PNTz4TF4 relative to a non-fluorinated polymer, PNTz4T. As expected from the deep E_{HS}, V_{OC}s of the PNTz4TF2 and PNTz4TF4 cells were improved to 0.82 V and 0.93 V, respectively, relative to that of the PNTz4T cell (0.71 V). As a result, the E_{loss}s of the PNTz4TF2 and PNTz4TF4 cells were reduced to 0.78 eV and 0.69 eV, respectively, from that of the PNTz4T cell (0.82 eV). Compared with the PNTz4T cell, the PNTz4TF4 cell exhibited ~6.5% PCE and lower J_{SC} and FF, whereas the PNTz4TF2 cell had ~10.5% PCE with similar J_{SC} and lower FF. The PCE of the PNTz4TF2 cell is higher than that of the PNTz4T cell (~10.1%) and is significantly high for single-junction PSCs. The charge generation study revealed that charge dissociation is the dominant factor for the difference in J_{SC} among these cells. The bimolecular recombination study demonstrated that recombination was increased as the number of fluorine atoms was increased, and this was likely the cause of the lower FF of the PNTz4TF2 and PNTz4TF4 cells than the PNTz4T cell. These behaviors were well correlated with the difference in crystallinity and backbone orientation investigated by 2D GIXD measurements: crystallinity was low particularly in PNTz4TF4, and the ratio of the face-on orientation was reduced in PNTz4TF2 and PNTz4TF4 compared to that in PNTz4T. However, it should be mentioned that the poor ordering structures in the fluorinated polymers likely originate in their low solubility, probably owing to the enhanced backbone coplanarity as predicted by the computation. Thus, we believe that by tuning the solubility and optimizing the fabrication process, the photovoltaic performance of the solar cells based on PNTz4TF2 and PNTz4TF4 would be further increased. These results demonstrate that there is still room for improvement of the efficiency of PSCs.

Associated Content

This material is available free of charge via the Internet at http://pubs.acs.org.

Supporting Information

The Supporting Information is available free of charge on the ACS Publications website.

Detailed experimental procedures and characterization of monomers and polymers, as well as additional figures and tables

Author Information

Corresponding Author: ohkita@photo.polym.kyoto-u.ac.jp, itaru.osaka@riken.jp

Notes: The authors declare no competing financial interest.

Acknowledgments

This work was supported by KAKENHI (16H04196 and 26288007) from Japan Society for the Promotion of Science, and the Advanced Low Carbon Technology Research and Development (ALCA) Program from Japan Science and Technology Agency. Elemental analysis and high-resolution mass spectrometry were carried out at the Materials Characterization Support Unit of RIKEN, Advanced Technology Support Division. 2D GIXD experiments were performed at BL46XU of SPring-8 with the approval of the Japan Synchrotron Radiation Research Institute (Proposals 2014B1915 and 2015B1904). The authors thank Dr. M. Abe of Nippon Kayaku Co. Ltd. for the TG analysis.

References

(1) Brabec, C.; Scherf, U.; Dyakonov, V. *Organic photovoltaics: Materials, Device Physics, and Manufacturing Technologies, 2nd Edition*; Wiley-VCH: Weinheim, Germany, 2014.

(2) Günes, S.; Neugebauer, H.; Sariciftci, N. S. *Chem. Rev.* **2007**, *107*, 1324.

(3) Brabec, C. J.; Gowrisanker, S.; Halls, J. J. M.; Laird, D.; Jia, S.; Williams, S. P. *Adv. Mater.* **2010**, *22*, 3839.

(4) Li, G.; Zhu, R.; Yang, Y. *Nat. Photon.* **2012**, *6*, 153.

(5) Kaltenbrunner, M.; White, M. S.; Głowacki, E. D.; Sekitani, T.; Someya, T.; Sariciftci, N. S.; Bauer, S. *Nat. Commun.* **2012**, *3*, 770.

(6) Chen, C.-C.; Dou, L.; Zhu, R.; Chung, C.-H.; Song, T.-B.; Zheng, Y. B.; Hawks, S.; Li, G.; Weiss, P. S.; Yang, Y. *ACS Nano* **2012**, *6*, 7185.

(7) Betancur, R.; Romero-Gomez, P.; Martinez-Otero, A.; Elias, X.; Maymo, M.; Martorell, J. *Nat. Photon.* **2013**, *7*, 995.

(8) Liu, Y.; Zhao, J.; Li, Z.; Mu, C.; Ma, W.; Hu, H.; Jiang, K.; Lin, H.; Ade, H.; Yan, H. *Nat. Commun.* **2014**, *5*, 5293.

(9) Vohra, V.; Kawashima, K.; Kakara, T.; Koganezawa, T.; Osaka, I.; Takimiya, K.; Murata, H. *Nat. Photon.* **2015**, *9*, 403.

(10) Zhao, W.; Qian, D.; Zhang, S.; Li, S.; Inganäs, O.; Gao, F.; Hou, J. *Adv. Mater.* **2016**, *28*, 4734.

(11) Mühlbacher, D.; Scharber, M.; Morana, M.; Zhu, Z.; Waller, D.; Gaudiana, R.; Brabec, C. *Adv. Mater.* **2006**, *18*, 2884.

(12) Boudreault, P.-L. T.; Najari, A.; Leclerc, M. *Chem. Mater.* **2011**, *23*, 456.

(13) Facchetti, A. *Chem. Mater.* **2011**, *23*, 733.

(14) Beaujuge, P. M.; Fréchet, J. M. J. *J. Am. Chem. Soc.* **2011**, *133*, 20009.

(15) Thompson, B. C.; Fréchet, J. M. J. *Angew. Chem. Int. Ed.* **2008**, *47*, 58.

(16) Piliego, C.; Holcombe, T. W.; Douglas, J. D.; Woo, C. H.; Beaujuge, P. M.; Fréchet, J. M. J. *J.*

Am. Chem. Soc. **2010**, *132*, 7595.

(17) Osaka, I.; Takimiya, K. *Polymer* **2015**, *59*, A1.

(18) Osaka, I.; Saito, M.; Koganezawa, T.; Takimiya, K. *Adv. Mater.* **2014**, *26*, 331.

(19) Wang, M.; Hu, X.; Liu, P.; Li, W.; Gong, X.; Huang, F.; Cao, Y. *J. Am. Chem. Soc.* **2011**, *133*, 9638.

(20) Osaka, I.; Shimawaki, M.; Mori, H.; Doi, I.; Miyazaki, E.; Koganezawa, T.; Takimiya, K. *J. Am. Chem. Soc.* **2012**, *134*, 3498.

(21) Osaka, I.; Abe, T.; Shimawaki, M.; Koganezawa, T.; Takimiya, K. *ACS Macro Lett.* **2012**, *1*, 437.

(22) Yang, T.; Wang, M.; Duan, C.; Hu, X.; Huang, L.; Peng, J.; Huang, F.; Gong, X. *Energy Environ. Sci.* **2012**, *5*, 8208.

(23) Osaka, I.; Kakara, T.; Takemura, N.; Koganezawa, T.; Takimiya, K. *J. Am. Chem. Soc.* **2013**, *135*, 8834.

(24) Kawashima, K.; Miyazaki, E.; Shimawaki, M.; Inoue, Y.; Mori, H.; Takemura, N.; Osaka, I.; Takimiya, K. *Polym. Chem.* **2013**, *4*, 5224.

(25) Kawashima, K.; Tamai, Y.; Ohkita, H.; Osaka, I.; Takimiya, K. *Nat. Commun.* **2015**, *6*, 10085.

(26) Zhou, H.; Yang, L.; Stuart, A. C.; Price, S. C.; Liu, S.; You, W. *Angew. Chem. Int. Ed.* **2011**, *50*, 2995.

(27) Price, S. C.; Stuart, A. C.; Yang, L.; Zhou, H.; You, W. *J. Am. Chem. Soc.* **2011**, *133*, 4625.

(28) Stuart, A. C.; Tumbleston, J. R.; Zhou, H.; Li, W.; Liu, S.; Ade, H.; You, W. *J. Am. Chem. Soc.* **2013**, *135*, 1806.

(29) Jo, J. W.; Jung, J. W.; Wang, H.-W.; Kim, P.; Russell, T. P.; Jo, W. H. *Chem. Mater.* **2014**, *26*, 4214.

(30) Liang, Y.; Feng, D.; Wu, Y.; Tsai, S. T.; Li, G.; Ray, C.; Yu, L. *J. Am. Chem. Soc.* **2009**, *131*, 7792.

(31) Gao, Y.; Zhang, X.; Tian, H.; Zhang, J.; Yan, D.; Geng, Y.; Wang, F. *Adv. Mater.* **2015**, *27*, 6753.

(32) Fei, Z.; Boufflet, P.; Wood, S.; Wade, J.; Moriarty, J.; Gann, E.; Ratcliff, E. L.; McNeill, C. R.; Sirringhaus, H.; Kim, J.-S.; Heeney, M. *J. Am. Chem. Soc.* **2015**, *137*, 6866.

(33) Sakamoto, Y.; Komatsu, S.; Suzuki, T. *J. Am. Chem. Soc.* **2001**, *123*, 4643.

(34) Kawabata, K.; Osaka, I.; Nakano, M.; Takemura, N.; Koganezawa, T.; Takimiya, K. *Adv. Electron. Mater.* **2015**, *1*, 1500039.

(35) Yoshida, H. *Chem. Phys. Lett.* **2012**, *539–540*, 180.

(36) Yoshida, H. *J. Electron Spectrosc. Relat. Phenom.* **2015**, *204, Part A*, 116.

(37) D'Andrade, B. W.; Datta, S.; Forrest, S. R.; Djurovich, P.; Polikarpov, E.; Thompson, M. E. *Org. Electron.* **2005**, *6*, 11.

(38) Melzer, C.; Koop, E. J.; Mihailetchi, V. D.; Blom, P. W. M. *Adv. Funct. Mater.* **2004**, *14*, 865.

(39) Rivnay, J.; Mannsfeld, S. C. B.; Miller, C. E.; Salleo, A.; Toney, M. F. *Chem. Rev.* **2012**, *112*, 5488.

(40) Duong, D. T.; Toney, M. F.; Salleo, A. *Phys. Rev. B* **2012**, *86*, 205205.

(41) Rogers, J. T.; Schmidt, K.; Toney, M. F.; Kramer, E. J.; Bazan, G. C. *Adv. Mater.* **2011**, *23*, 2284.

(42) Roe, R. J. *Methods of X-ray and Neutron Scattering in Polymer Science*; Oxford University Press: New York, 2000.

(43) Maurano, A.; Shuttle, C. G.; Hamilton, R.; Ballantyne, A. M.; Nelson, J.; Zhang, W.; Heeney, M.; Durrant, J. R. *J. Phys. Chem. C* **2011**, *115*, 5947.

(44) Credgington, D.; Durrant, J. R. *J. Phys. Chem. Lett.* **2012**, *3*, 1465.

(45) Hawks, S. A.; Deledalle, F.; Yao, J.; Rebois, D. G.; Li, G.; Nelson, J.; Yang, Y.; Kirchartz, T.; Durrant, J. R. *Adv. Energy Mater.* **2013**, *3*, 1201.

(46) Koster, L. J. A.; Mihailetchi, V. D.; Blom, P. W. M. *Appl. Phys. Lett.* **2006**, *88*, 052104.

(47) Tamai, Y.; Tsuda, K.; Ohkita, H.; Benten, H.; Ito, S. *Phys. Chem. Chem. Phys.* **2014**, *16*, 20338.

(48) Ohkita, H.; Tamai, Y.; Benten, H.; Ito, S. *IEEE J. Sel. Top. Quantum Electron.* **2016**, *22*, 4100612.

(49) Qi, B.; Wang, J. *Phys. Chem. Chem. Phys.* **2013**, *15*, 8972.

(50) Dibb, G. F. A.; Jamieson, F. C.; Maurano, A.; Nelson, J.; Durrant, J. R. *J. Phys. Chem. Lett.* **2013**, *4*, 803.

TOC graphic:

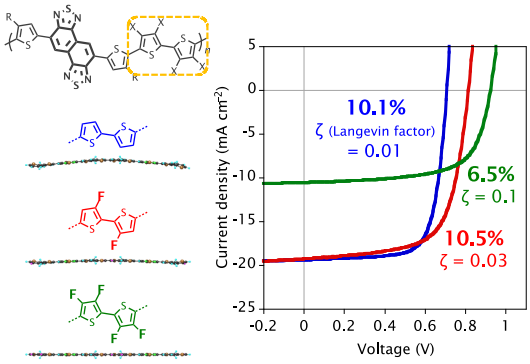
10.1%
ζ (Langevin factor)
= 0.01
6.5%
ζ = 0.1
10.5%
ζ = 0.03
Current density (mA cm-2)
Voltage (V)
5
0
-5
-10
-15
-20
-25
-0.2
0
0.2
0.4
0.6
0.8
1